

Some substrates of P-glycoprotein targeting β -amyloid clearance by quantitative structure-activity relationship (QSAR)/membrane-interaction (MI)-QSAR analysis

Tongyang Zhu, Jie Chen, Jie Yang*

State Key Laboratory of Pharmaceutical Biotechnology, Life College, Nanjing University, Nanjing, China
Email: luckyjyj@sina.com.cn

Received 28 April 2013; revised 29 May 2013; accepted 15 June 2013

Copyright © 2013 Tongyang Zhu *et al.* This is an open access article distributed under the Creative Commons Attribution License, which permits unrestricted use, distribution, and reproduction in any medium, provided the original work is properly cited.

ABSTRACT

The pathogenesis of Alzheimer's disease (AD) putatively involves a compromised blood-brain barrier (BBB). In particular, the importance of brain-to-blood transport of brain-derived metabolites across the BBB has gained increasing attention as a potential mechanism in the pathogenesis of neurodegenerative disorders such as AD, which is characterized by the aberrant polymerization and accumulation of specific misfolded proteins, particularly β -amyloid ($A\beta$), a neuropathological hallmark of AD. P-glycoprotein (P-gp), a major component of the BBB, plays a role in the etiology of AD through $A\beta$ clearance from the brain. Our QSAR models on a series of purine-type and propafenone-type substrates of P-gp showed that the interaction between P-gp and its modulators depended on Molar Refractivity, LogP, and Shape Attribute of drugs it transports. Meanwhile, another model on BBB partitioning of some compounds revealed that BBB partitioning relied upon the polar surface area, LogP, Balaban Index, the strength of a molecule combined with the membrane-water complex, and the changeability of the structure of a solute-membrane-water complex. The predictive model on BBB partitioning contributes to the discovery of some molecules through BBB as potential AD therapeutic drugs. Moreover, the interaction model of P-gp and modulators for treatment of multidrug resistance (MDR) indicates the discovery of some molecules to increase $A\beta$ clearance from the brain and reduce $A\beta$ brain accumulation by regulating BBB P-gp in the early stages of AD. The mechanism provides a new insight into the therapeutic strategy for AD.

Keywords: P-Glycoproteins; Quantitative

Structure-Activity Relationship; ATP-Binding Cassette Transporters; Multidrug Resistance; Blood-Brain Barrier

1. INTRODUCTION

Therapy for central nervous system (CNS) diseases requires drugs that can cross the blood-brain barrier (BBB) [1]. BBB not only maintains the homeostasis of the CNS, but also refuses many potentially important diagnostic and therapeutic agents from entering into the brain [2]. The pathological hallmarks of Alzheimer's disease (AD) are progressive brain atrophy and the accumulation of cortical senile plaques, formed by the aggregation of amyloid beta peptide ($A\beta$) [3], and neurofibrillary tangles (NFT), namely the self-assembly of hyperphosphorylated forms of the microtubule associated protein tau into fibers termed "paired helical filaments (PHFs)" [4,5]. The pathogenesis of AD's senile plaque and NFT lesions putatively involves a compromised BBB [6], which protects the brain against endogenous and exogenous compounds and plays an important part in the maintenance of the microenvironment of the brain [7]. The ability of drug permeating across BBB becomes critical in the development of new medicines, especially in the design of new drugs active in brain tissue. In particular, the importance of brain-to-blood transport of brain-derived metabolites across the BBB has gained increasing attention as a potential mechanism in the pathogenesis of neurodegenerative disorders such as Parkinson's disease (PD) [8] and AD characterized by the aberrant polymerization and accumulation of specific misfolded proteins, particularly $A\beta$. P-glycoprotein (P-gp or MDR1/ABCB1) is a 170-kDa transmembrane (TM) protein widely expressed from the epithelial cells of the intestine, liver, kidney, placenta, uterus, and testis to endothelial cells of the BBB [9]. It belongs to the ABC (ATP-binding cassette) transporter family and serves to pump exogenous substances

*Corresponding author.

out of the cells. The domain topology of P-gp consists of two homologous halves each consisting a TM domain preceding a cytosolic nucleotide binding domain. Each TM domain is composed of six TM α -helix segments involved in efflux as well as in drug binding [10]. The ABC transport protein P-gp, a major component of the BBB, mediates the efflux of $A\beta$ from the brain as well as is a major factor in mediating resistance to brain entry by numerous exogenous chemicals, including therapeutic pharmaceuticals [11]. P-gp plays a role in the etiology of AD through the clearance of $A\beta$ from the brain. Some drugs, such as rifampicin, dexamethasone, caffeine, verapamil, hyperforin, β -estradiol and pentylenetetrazole, were able to improve the efflux of $A\beta$ from the cells via P-gp up-regulation [12]. Meanwhile, some compounds have been shown to reverse the P-gp mediated multidrug resistance (MDR), including verapamil, adriamycin, cyclosporin, and dexverapamil [13]. Hartz *et al.* have shown that up-regulating P-gp in the early stages of AD has the potential to increase $A\beta$ clearance from the brain and reduce $A\beta$ brain accumulation by a transgenic mouse model of AD (hAPP-overexpressing mice) [14]. Abuznait *et al.* have also elucidated the impact of P-gp up-regulation on the clearance of $A\beta$ [12], which indicated that targeting $A\beta$ clearance via P-gp up-regulation was effective in slowing or halting the progression of AD and there was the possibility of P-gp as a potential therapeutic target for AD.

P-gp at the BBB functions as an active efflux pump by extruding a substrate from the brain, which is important for maintaining loco-regional homeostasis in the brain and protection against toxic compounds [8]. P-gp is also discovered in various resistant tumor cells and expressed widely in many normal tissues and plays a very important role in drug ADME-Tox (absorption, distribution, metabolism, excretion, and toxicity). MDR is a matter of growing concern in chemotherapy. Cells which express the MDR phenotype can over-express efflux transporters after exposure to a single agent. As a result, these cells become resistant to the selective agent and cross-resistant to a broad spectrum of structurally and functionally dissimilar drugs. The drug efflux pump P-gp has been shown to promote MDR in tumors as well as to influence ADME properties of drug candidates [15]. P-gp is expressed at the BBB, the blood-cerebrospinal fluid barrier, and the intestinal barrier, thus modulating the absorption and excretion of xenobiotics across these barriers. P-gp and its ligands (substrates and inhibitors) are therefore extensively studied both with respect to reversing MDR in tumors and for modifying ADME-Tox properties of drug candidates, such as CNS active agents [15]. P-gp possesses broad substrate specificity and the substrates include members of many clinically important therapeutic drug classes, including anti-HIV protease inhibitors, calcium channel blockers used in the treatment of angina,

hypertension, antibiotics and cancer chemotherapeutics [16]. In this active efflux process, energy originating from ATP hydrolysis is directly consumed. Because of such a wide distribution of P-gp, if a drug such as quinine or verapamil inhibits the function of P-gp, it will also inhibit the excretion of digoxin by P-gp's leading to increased plasma levels and toxicity due to digoxin. It is believed to be an important protective mechanism against environmental toxins. Since the function of P-gp always results in the lack of intracellular levels of the drug necessary for effective therapy, the overexpression of P-gp in certain malignant cells is always associated with MDR phenotype [17]. Although a low resolution structure of P-gp is obtained, its physiological function and mechanisms of MDR modulation are still not very clear [18]. It is well known that a large number of structurally and functionally diverse compounds act as substrates or modulators of P-gp, including calcium and sodium channel blockers, calmodulin antagonists and structural analogues, protein kinase C inhibitors, steroidal and structurally related compounds, indole alkaloids, cyclic peptides and macrolide compounds, flavanoids and miscellaneous compounds [19], which mostly share common structural features, such as aromatic ring structures and high lipophilicity. Some of them possess MDR reversing activity while only a small number of them have entered clinical study. Classification of candidate drugs as substrates or inhibitors of the carrier protein is crucial in drug development [20].

On the other hand, the prerequisite to cure neurological disorders is that the drug distribution in CNS can reach effectively therapeutic concentrations [2]. Usually, the high BBB penetration is needed for drugs that activate in brain. The molecule negotiating the BBB must go through cellular membranes comprised of a lipid bilayer. Until now, it is widely accepted that interaction of compounds with P-gp is a complex process and at this time the details of its mechanism of action are still the subject of hot debate. Although the experimental analysis of drug permeability is essential, the procedure of experiment is time consuming and complicated, a theoretical model of drug permeability is effective to give predictions. Membrane-interaction (MI)-QSAR (quantitative structure-activity relationship) method is a structure-based design methodology combined with classic intramolecular QSAR analysis to model chemically and structurally diverse compounds interacting with cellular membranes. Our modified MI-QSAR method that combines QSAR with solute-membrane-water complex simulating the BBB environment is more close to the body condition than MI-QSAR and possesses higher ability to predict organic compounds across BBB [21]. There are several critical assumptions considered that can influence validity and correctness of any QSAR study as follows: the same

mechanism of action of all studied analogs; a comparable manner of their binding to the receptor; correlation of binding to the interaction energies; correlation of measured biological activities to the binding affinities [22]. All the accuracy answer and research based on the above questions above may guarantee that proper and reliable relationships are obtained. However, different mechanisms and different binding sites may be involved in the case of MDR modulators. Several screening assays can help in the identification of substrates and inhibitors although they have both advantages and drawbacks, such as cytotoxicity assays [23], inhibition of efflux assays [16], P-gp-ATPase activation assays, and drug transport assays [24].

The goal of a QSAR study is to find a means of predicting the activity of a new compound. If possible, a desirable goal is the understanding of the biology and chemistry that give rise to that activity and the consequential possibility of reengineering the compound to remove or enhance that activity. One successful example is the transformation of nalidixic acid with the help of QSAR into an important family of drug: the quinolone carboxylates, such as norfloxacin, fleroxacin, ciprofloxacin, and levofloxacin [25]. Since the method was established in the 1960s, QSAR equations have been used to describe the biological activities of thousands of different drugs and drug candidates [26]. The method definitely provides a more accurate way to synthesize or filtrate the new chemical compounds. At last, the final destination is to degrade the cost of research and manufacture. To date, so many methods have been used in QSAR study and some of them have got successful results. There are general methods used in the literatures these years, such as multiple linear regression (MLR) method, partial least square regression (PLSR) [18], MI-QSAR analysis [21], 3D QSAR [27], and artificial neural network (ANN) [28]. In order to get more accurate results and QSAR models, we have used two different analyses: MLR and PLSR. Moreover, we focus on constructing theoretical models of the interaction between organic compounds and P-gp as well as the predictive models of BBB partitioning of organic compounds on the basis of QSAR analysis and MI-QSAR analysis.

2. MATERIALS AND METHODS

2.1. P-Glycoprotein Ligands

Building of some compounds. 36 purine derivatives were selected and used in QSAR analysis (**Table 1**) [29]. These compounds were divided into two sets: the training set and the test set. The study of the MDR-reversing properties of these derivatives was carried out *in vitro* on P388/VCR-20 cells, a murine leukemia cell line whose resistance was induced by vincristine (VCR), and KB-A1 cells, a human epidermoid carcinoma cell line whose

resistance was induced by adriamycin (ADR). The compounds were tested at four concentrations (0.5 - 5 μ M) in association with VCR (P388/VCR-20 cells) or ADR (KB-A1 cells). In this test, MDR ratio in P388/VDR-20 and KB-A1 *in vitro* was used as biological activity for the

whole dataset, namely
$$\text{MDR}_{\text{ratio}} = \frac{\text{IC}_{50}(\text{CD})}{\text{IC}_{50}(\text{CD} + \text{mod})}$$
.

Here "CD" is the abbreviation for cytotoxic drug (such as VCR and ADR) in cytotoxicity assays, and "mod" means modulators. It is defined as ratio between the IC_{50} values (concentration that inhibits the growth of MDR cells by 50%) of the cytotoxic agent in absence and presence of relatively nontoxic concentration of the modifier [23]. Most often the IC_{50} for several concentration of a cytotoxic drug is evaluated in the presence and absence of a nontoxic concentration of a P-gp modifier. In this assay modulators that interacted with P-gp and thus reduced the efflux of the cytotoxic compounds would increase the apparent toxicity of the cytotoxic compound [16]. The IC_{50} data were based on a general assessment of cytotoxicity and thus might account for more than one acting mechanism in the resistant cells used [16]. Furthermore, it is well known that the MDR ratio for any given compound can vary greatly depending on the cell type used for the assay as well as the intrinsic cytotoxicity of the compounds used. The data is also dependent on the concentration of the P-gp substrates or modulators used in the studies [30].

Similarly, another 21 propafenone analogs were selected from the literature of Diethart Schmid *et al.* and used in QSAR analysis (**Table 2**) [31]. In this test K_a of P-gp ATPase in the adriamycin-resistant subline CCRF ADR5000 was used as biological activity for the whole dataset [31]. The assays were performed based on the colorimetric determination of inorganic phosphate released by the hydrolysis of ATP. **Table 2** shows all the structures and the experimental biological activity value.

Finally, all two-dimensional (2D) structures of these compounds mentioned above were constructed using the chemical drawing software ChemDraw 8.0 and prepared for the next calculation.

Calculation of some descriptors. Molecular descriptors are "numbers that characterize a specific aspect of the molecular structure" [32]. There are some molecular descriptors used in QSAR studies as follows: physicochemical properties (*i.e.* hydrophobicity, aqueous solubility, molecular electronegativity, and molecular refractivity), quantum chemical parameters (e.g. atomic charges, energies of HOMO (highest occupied molecular orbital) and LUMO (lowest unoccupied molecular orbital)) [33], topological indexes (such as molecular connectivity indexes) [34], and other 3D descriptors. Molecular descriptors were mostly calculated by the commercial soft-

Table 1. The structures and MDR ratios of 35 purine derivatives in the training/test sets.

No.	Structure	<i>In vitro</i> reversal fold reversion (MDR ratio)		No.	Structure	<i>In vitro</i> reversal fold reversion (MDR ratio)	
		P388/VCR-20	KB-A1			P388/VCR-20	KB-A1
A1		50	171	A19		36	49
A2		78	278	A20		70	214
A3		75	238	A21		35	113
A4		53	236	A22		133	200
A5		236	160	A23		193	189
A6		93	208	A24		24	142
A7		124	102	A25		13	6

Continued

A8		30	120	A26		24	9
A9		57	75	A27		84	406
A10		108	136	A28		57	68
A11		37	44	A29		108	723
A12		15	83	A30		27	370
A13		78	272	A31		288	210
A14		56	147	A32		59	121
A15		75	152	A33		71	499
A16		51	209	A34		13	264

Continued

A17		70	171	A35		3	5
A18		129	156				

Note: Ratio of IC_{50} (cytotoxic alone (VCR for P388/VCR-20, ADR for KB-A1 cells))/ IC_{50} (cytotoxic + modulator) (1 μ M in association with VCR or 2.5 μ M in association with ADR) [29].

Table 2. The structures and K_a values and LogP of 18 propafenone analogs in the training/test sets.

No.	Structure	K_a (μ M/L)	LogP	No.	Structure	K_a (μ M/L)	LogP
A36		3.34	3.39	A45		1.53	4.3
A37		5.3	3.62	A46		1.47	4.93
A38		2.59	3.67	A47		0.55	5.2
A39		122	1.42	A48		7.64	4.25

Continued

A40		0.36	4.93	A49		12.2	4.52
A41		6.13	2.67	A50		2.26	4.88
A42		120	0.94	A51		10.5	2.38
A43		18.5	2.54	A52		12.8	3.94
A44		1.01	3.98	A53		4.15	4.93

ware packages Chemoffice Chem3D Ultra 8.0, involving molecular mechanism parameters (Stretch-Bend Energy (E_{stretch}), Bending Energy (E_{bend}), Torsion Energy (E_{torsion}), Total Energy (E_{total}), van der Waals Energy (E_{VDW}), etc), quantum chemistry parameters (*i.e.* Electronic Energy

($E_{\text{electronic}}$), HOMO Energy (E_{HOMO}) and LUMO Energy (E_{LUMO})), hydrophobic parameters (such as ClogP), stereo parameters (eg. E_s , Balaban Index (BI), Connolly Accessible Area (CAA), Molecular Weight (MW), Shape Attribute (ShA), Total Connectivity (T_{con}), and Wiener

Index (WI)), thermodynamic parameters, including Henry's Law Constant (H), Hydration Energy (E_{hyd}), Logarithm of partition coefficient in n-octanol/water (LogP), Molar Refractivity (MR), and molecular polar surface area (PSA) that defined as the surface area (\AA^2) occupied by polar atoms, usually oxygen, nitrogen and hydrogen attached to them, which will restrict molecule penetration into the membranes [2]. The other properties involved in number of hydrogen bond acceptor (NBA) and number of hydrogen bond donor (NBD).

The energy parameters root in the results of molecular mechanism and molecular dynamics. The total energy of a system expressed as follows [35]: $E_{\text{total}} = E_{\text{valence}} + E_{\text{crossterm}} + E_{\text{nonbond}}$. Here, the valence interactions includes bond stretching (bond), valence angle bending (angle), dihedral angle torsion (torsion), and inversion, also called out-of-plane interactions (oop) terms, which are part of nearly all forcefields for covalent systems. A Urey-Bradley term (UB) may be used to account for interactions between atom pairs involved in 1 - 3 configurations (*i.e.*, atoms bound to a common atom): $E_{\text{valence}} = E_{\text{bond}} + E_{\text{angle}} + E_{\text{torsion}} + E_{\text{oop}} + E_{\text{UP}}$. Modern (second-generation) forcefields generally achieve higher accuracy by including cross terms to account for such factors as bond or angle distortions caused by nearby atoms. Crossterms can include the following terms: stretch-stretch, stretch-bend-stretch, bend-bend, torsion-stretch, torsion-bend-bend, bend-torsion-bend, stretch-torsion-stretch. The interaction energy between non-bonded atoms is accounted by van der Waals (VDW), electrostatic (Coulomb), and hydrogen bond (hbond) terms in some older forcefields. $E_{\text{non-bond}} = E_{\text{VDW}} + E_{\text{Coulomb}} + E_{\text{hbond}}$. Restraints that can be added to an energy expression include distance, angle, torsion, and inversion restraints. Restraints are useful for information on restraints and their implementation and use if you are interested in only part of a structure, and so is the documentation for the particular simulation engine.

These descriptors were calculated using Chemoffice Chem3D Ultra 8.0 and Hyperchem 7.5 as follows: 1) the structures of the compounds were drawn in ChemDraw 8.0 and sequentially changed to 3D structures by Chem3D; 2) the chosen compounds were minimized by molecular mechanism using MM2 force field with RMS (root mean square) gradient of 0.100; and 3) under the menu of Analyze-compute properties, the properties were selected to calculate and finally every descriptor value of each compound was gotten.

QSAR models. QSAR models of some purine derivatives (Table 1) were achieved by partial sum of squares for regression with software SPSS 10.0. A training set of 26 structurally diverse purine derivatives are measured is used to construct QSAR models. The QSAR models are optimized using MLR fitting and stepwise method (Eqs.1-5). A test set of five compounds is evaluated using the

QSAR models as part of a validation process. Take MDR ratio *in vitro* in P388/VDR cell lines as dependent variable and molecule descriptors as independent variable. With the aid of Virtual Computational Chemistry Laboratory software [20], QSAR modeling was constructed by PLSR (Eq.6).

Similarly, a training set of 18 structurally diverse propafenone analogs (Table 2) are measured is used to construct QSAR models. The QSAR models are optimized using MLR fitting and stepwise method (Eqs.7-11). Another QSAR modeling was constructed by PLSR (Eq.12). A test set of five compounds is evaluated using the QSAR models as part of a validation process.

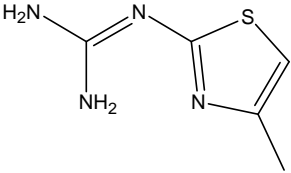
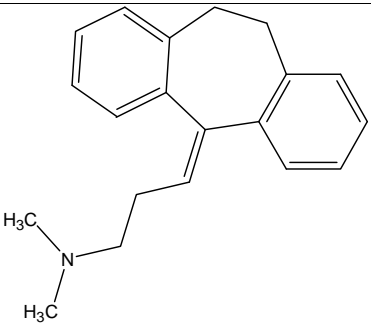
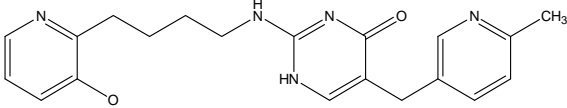
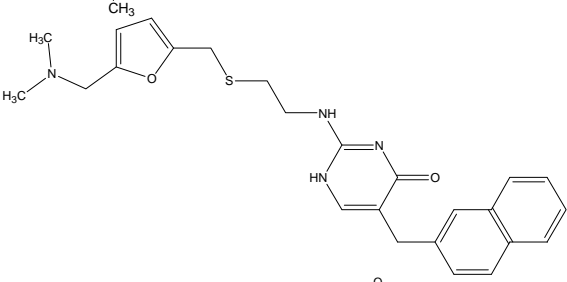
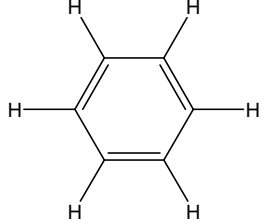
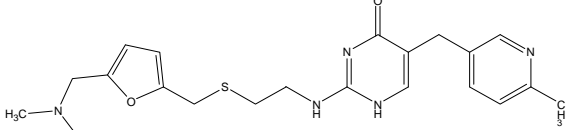
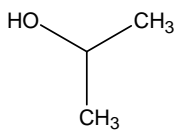
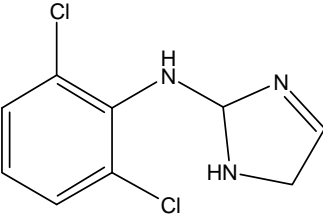
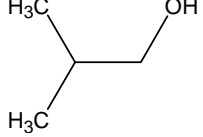
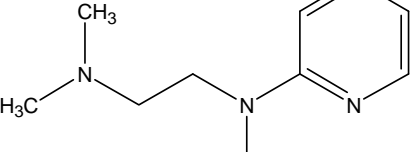
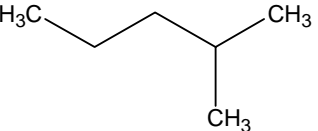
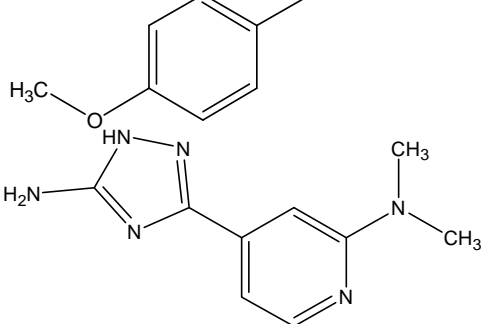
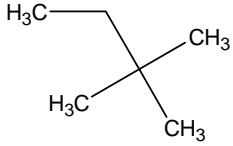
2.2. Blood-Brain-Barrier

Data. 37 organic compounds [36,37] were elected to compose a train set while another 8 organic compounds were acted as a test set (Table 3). The dependent variable is the logarithm of the BBB partition coefficient, $\log \text{BB} = \log(C_{\text{brain}}/C_{\text{blood}})$, where C_{brain} is the concentration of the test compound in the brain, and C_{blood} is the concentration of the test compound in blood. Experimental values of $\log \text{BB}$ published to date lie approximately between -2.00 to $+1.04$. Compounds with $\log \text{BB}$ values of >0.30 are readily distributed to the brain whereas compounds with values <-1.00 are poorly distributed to the brain. Building of all these compounds was performed using the Build modules of Hyperchem 7.5. The geometry of these compounds was optimized using the Amber 94 force field in gas state and sequentially placed at a periodic solvent box with a volume of $16 \times 10 \times 18 \text{\AA}^3$, which included 96 water molecules. Here, temperature is 300°K and pressure is 1 standard atmosphere. Then, the compounds in water were minimized by the above method and simulated by Monte Carlo method.

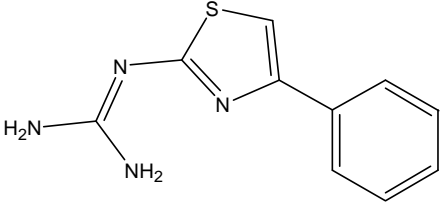
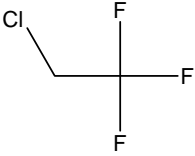
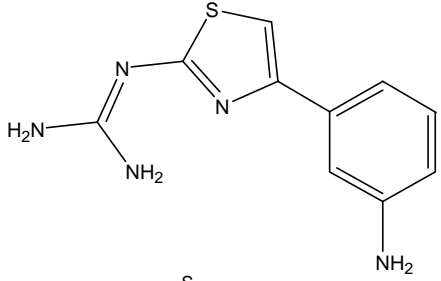
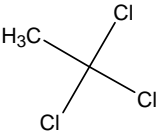
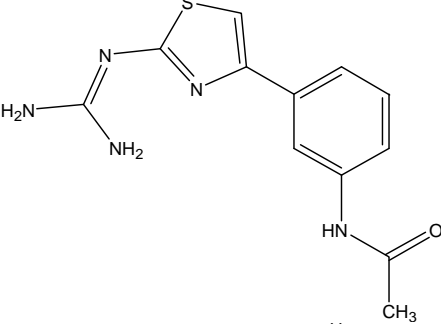
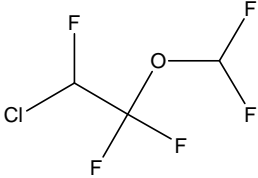
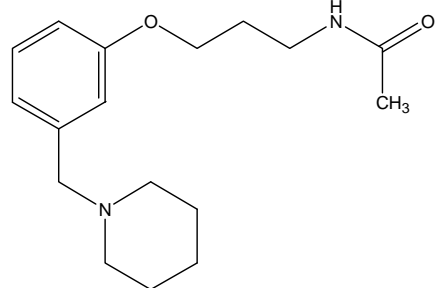
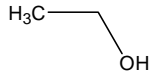
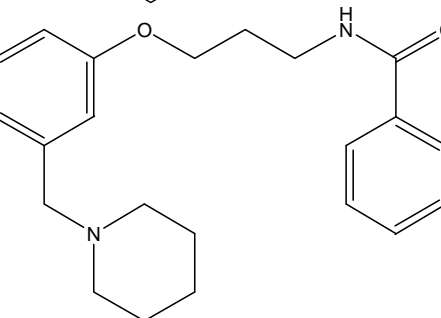
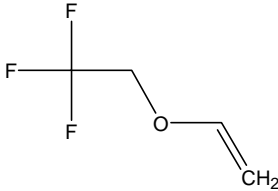
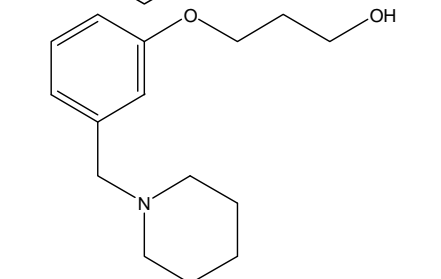
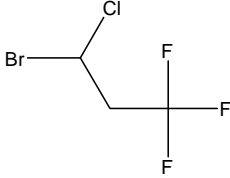
Molecular modeling of a dimyristoylphosphatidylcholine (DMPC) monolayer membrane complex with a layer of water. A model of DMPC monolayer membrane composed of 25 DMPC molecules ($5 \times 5 \times 1$) was constructed using Material Studio and minimized for 200 steps with the smart minimizer. Here, the parameter of the single crystal of DMPC with $a = 8 \text{\AA}$, $b = 8 \text{\AA}$, and $\gamma = 96.0^\circ$ resulted in each lipid molecule with an average area of 64\AA^2 similar to Stouch's research results [38]. Moreover, a layer of water ($40 \times 40 \times 10 \text{\AA}^3$) including 529 water molecules was added to the polar side of the DMPC monolayer membrane (Figure 1).

Molecular dynamic simulation of compound-DMPC-water complex models. A compound displaced a DMPC molecule in the DMPC monolayer membrane at three different positions (upper, center or lower) to form each solute-membrane-water complex. Molecular dynamic

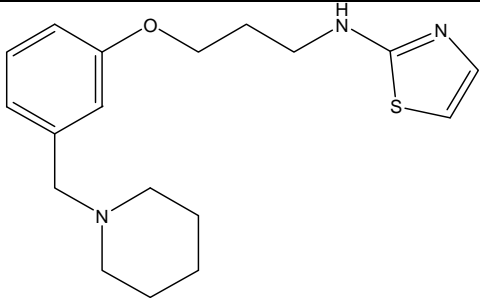
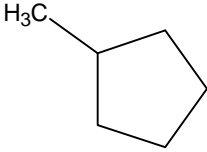
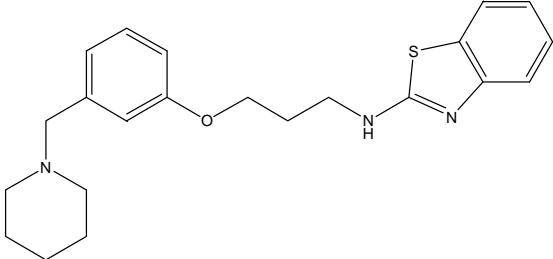
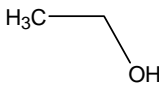
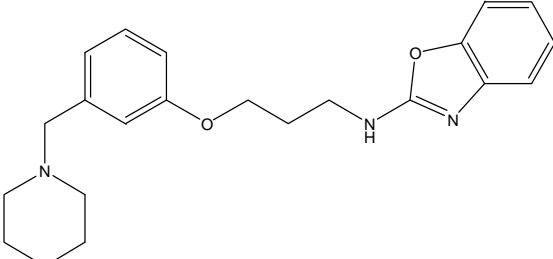
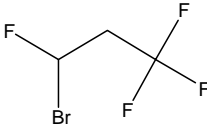
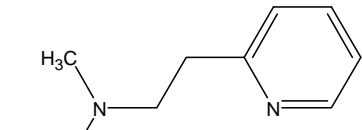
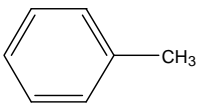
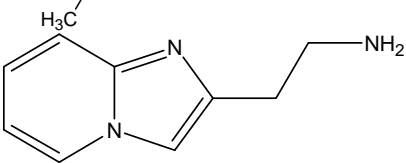
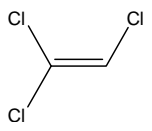
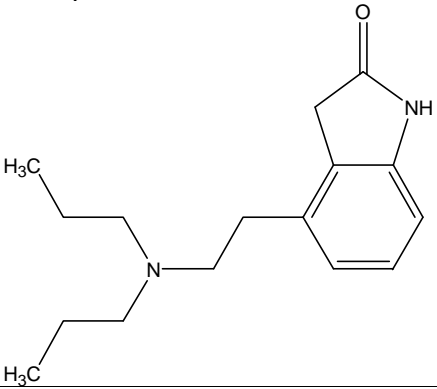
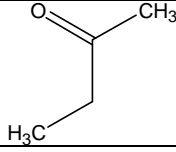
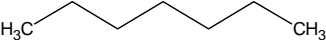
Table 3. The structures and LogBB values of some compounds in the training/test sets.

No	Structure	LogBB	No	Structure	LogBB
Training set					
B1		-0.04	B20		0.85
B2		-2.00	B21		0.03
B3		-1.30	B22		0.37
B4		-1.06	B23		-0.15
B5		0.11	B24		-0.17
B6		0.49	B25		0.97
B7		-1.17	B26		1.04

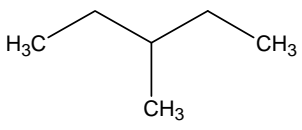
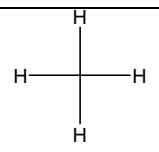
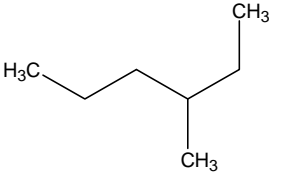
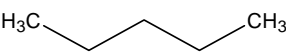
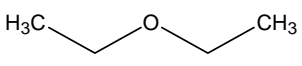
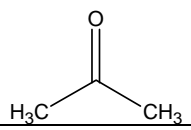
Continued

B8		-0.18	B27		0.08
B9		-1.15	B28		0.40
B10		-1.57	B29		0.24
B11		-0.46	B30		-0.16
B12		-0.24	B31		0.13
B13		-0.02	B32		0.35

Continued

B14		0.44	B33		0.93
B15		0.14	B34		-0.16
B16		0.22	B35		0.27
B17		-0.06	B36		0.37
B18		-1.40	B37		0.34
B19		0.25			
Test set					
T1		-0.08	T5		0.81

Continued

T2		1.01	T6		0.04
T3		0.90	T7		0.76
T4		0.00	T8		-0.15

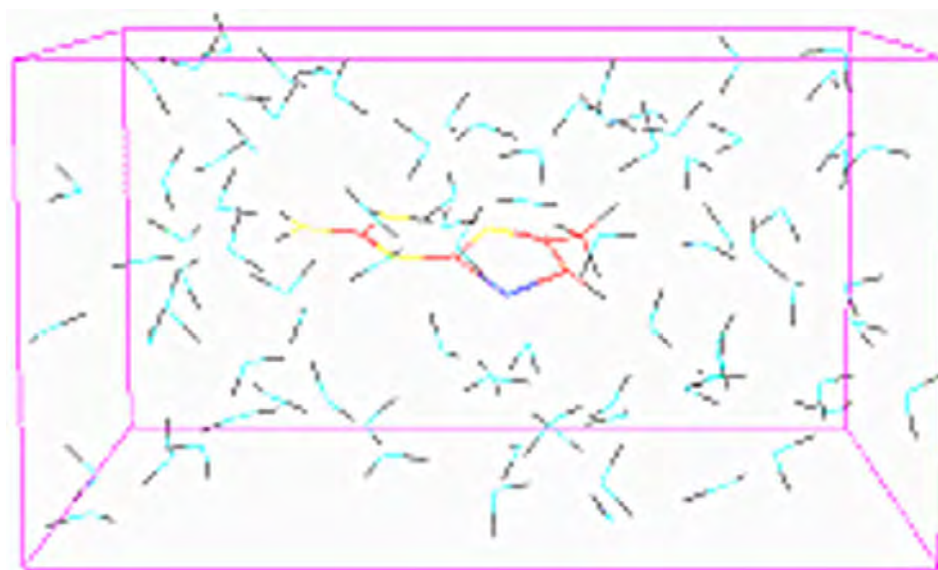


Figure 1. Compound B1 colored by atom-type in water and the solvent box defined in Monte Carlo simulation.

simulation of the complex was performed for 1000 steps by Discover module with Materials Studios, using Compass force field. Here, the 3D volume was restricted to a border of $X = 40 \text{ \AA}$, $Y = 40 \text{ \AA}$, $Z = 91.76 \text{ \AA}$, and $\gamma = 96.0^\circ$.

QSAR model of BBB partitioning of some compounds. MI-QSAR model of a training set of 37 compounds through BBB were achieved by partial sum of squares for regression with SPSS. Molecular dynamics simulations were used to determine the explicit interaction of each compound with a model of DMPC monolayer membrane complexed with a layer of water. An additional set of intramolecular solute descriptors were computed and considered in the trial pool of descriptors for building MI-QSAR models. The MI-QSAR models were optimized using multidimensional linear regression fitting and stepwise method. The MI-QSAR models were then evaluated by a test set of 8 compounds.

3. RESULTS

3.1. QSAR Analysis Based on MDR Ratio in P388/VDR-20 and KB-A1 *in Vitro*

MDR ratio of compounds *in vitro* in KB-A1/ADR cell lines was taken as the dependent variable. A training set of 26 compounds (**Table 4**) was used to construct QSAR models. The QSAR models were optimized using MLR fitting and stepwise method by SPSS (**Eqs.1-5**). A test set of 5 compounds (A27-A31) was evaluated using the models as part of a validation process (**Figure 2** upper, **Table 5**).

Similarly, MDR ratio of compounds *in vitro* in P388/VDR cell lines acted as the dependent variable. With the aid of Virtual Computational Chemistry Laboratory software (<http://vcclab.org>) [20], some QSAR models were constructed by PLSR (**Eq.6**, **Figure 2** down). **Table 6** shows the calculated descriptors mentioned above and

Table 4. The molecular descriptors of some compounds related to MDR ratios in the training/test sets.

No.	LogMR	ShA	BI	LogP	E _{hyd} (kcal/mol)	No.	LogMR	ShA	BI	LogP	E _{hyd} (kcal/mol)
Training set											
A1	1.20	37.03	2,662,570	3.33	-3.56	A14	1.22	39.02	3,358,755	1.48	-19.64
A2	1.18	35.03	2,440,928	2.59	-13.71	A15	1.22	39.02	3,358,755	1.48	-19.71
A3	1.22	40.02	3,649,082	1.14	-16.23	A16	1.20	37.03	2,662,570	2.13	-15.99
A4	1.14	32.03	1,669,953	2.21	-13.54	A17	1.202	37.03	2,662,570	2.13	-16.23
A5	1.22	39.02	3,358,755	1.33	-19.71	A18	1.202	37.03	2,662,570	2.13	-15.95
A6	1.20	37.03	2,662,570	2.13	-16.22	A19	1.18	37.03	3,091,919	1.61	-15.9
A7	1.22	40.02	3,491,392	0.76	-17.67	A20	1.23	41.02	4,008,723	0.76	-17.36
A8	1.20	37.03	2,662,570	2.28	-16.3	A21	1.14	32.03	1,651,352	1.9	-13.79
A9	1.24	42.02	4,491,514	1.29	-16.34	A22	1.22	39.02	3,324,212	1.33	-20.06
A10	1.24	41.02	4,055,919	0.99	-19.77	A23	1.20	37.03	2,634,052	2.13	-15.77
A11	1.18	36.03	2,271,976	1.41	-17.73	A24	1.19	36.03	2,246,188	2.13	-16.15
A12	1.19	36.03	2,271,976	2.13	-16.17	A25	1.15	35.03	2,244,801	1.71	-14.88
A13	1.15	33.03	1,900,460	2.28	-13.57	A26	1.15	35.03	2,271,261	1.71	-15.03
Test set											
A27	1.19	37.03	2,662,570	1.41	-18.09	A30	1.25	41.02	3,977,672	2.98	-13.52
A28	1.22	40.02	3,491,392	0.76	-17.61	A31	1.20	37.03	2,634,052	2.13	-15.95
A29	1.21	37.03	2,662,570	2.75	-15.55						

Table 5. The experimental values and the predictive values of MDR ratio of these compounds.

No.	MDR ratio (KB-A1)	Predictive values of MDR ratio					No.	MDR ratio (KB-A1)	Predictive values of MDR ratio				
		Eq.1	Eq.2	Eq.3	Eq.4	Eq.5			Eq.1	Eq.2	Eq.3	Eq.4	Eq.5
Training set													
A1	171	114.32	215.61	200.33	123.15	180.87	A14	147	151.94	151.04	171.02	173.75	144.79
A2	278	80.79	200.54	305.22	260.52	228.39	A15	152	150.27	140.09	157.75	159.16	130.87
A3	238	161.08	71.37	78.37	79.12	92.55	A16	209	115.64	233.15	217.87	209.32	197.83
A4	236	44.84	113.11	178.94	196.99	213.61	A17	171	115.64	233.15	217.87	209.32	193.94
A5	160	150.27	140.09	157.75	168.14	148.66	A18	156	116.97	252.09	236.91	229.26	219.10
A6	208	113.02	199.36	184.18	174.42	159.21	A19	49	81.98	22.31	33.79	29.47	25.56
A7	102	163.01	77.39	67.24	80.67	105.63	A20	214	198.44	93.91	119.73	132.46	165.76
A8	120	114.32	215.61	200.33	180.88	153.75	A21	113	42.69	80.90	121.41	145.60	174.56
A9	75	237.62	101.82	179.28	149.94	146.81	A22	200	150.27	140.09	149.67	160.44	139.02
A10	136	222.49	204.96	297.19	322.30	315.82	A23	189	113.02	199.36	176.36	167.80	160.14
A11	44	79.86	58.80	41.66	49.61	53.08	A24	142	92.42	159.30	116.68	117.52	112.54
A12	83	92.42	159.30	121.35	121.70	115.60	A25	6	52.12	10.08	9.16	8.45	8.02
A13	272	53.80	124.41	185.32	190.50	197.66	A26	9	52.12	10.08	9.53	8.76	8.16
Testset													
A27	406	99.21	81.97	70.98	80.61	81.67	A30	370	243.10	375.08	504.47	282.78	192.47
A28	68	163.01	77.39	67.24	80.67	106.16	A31	210	114.32	215.61	191.82	183.83	174.21
A29	723	125.69	411.51	400.76	323.36	248.59							

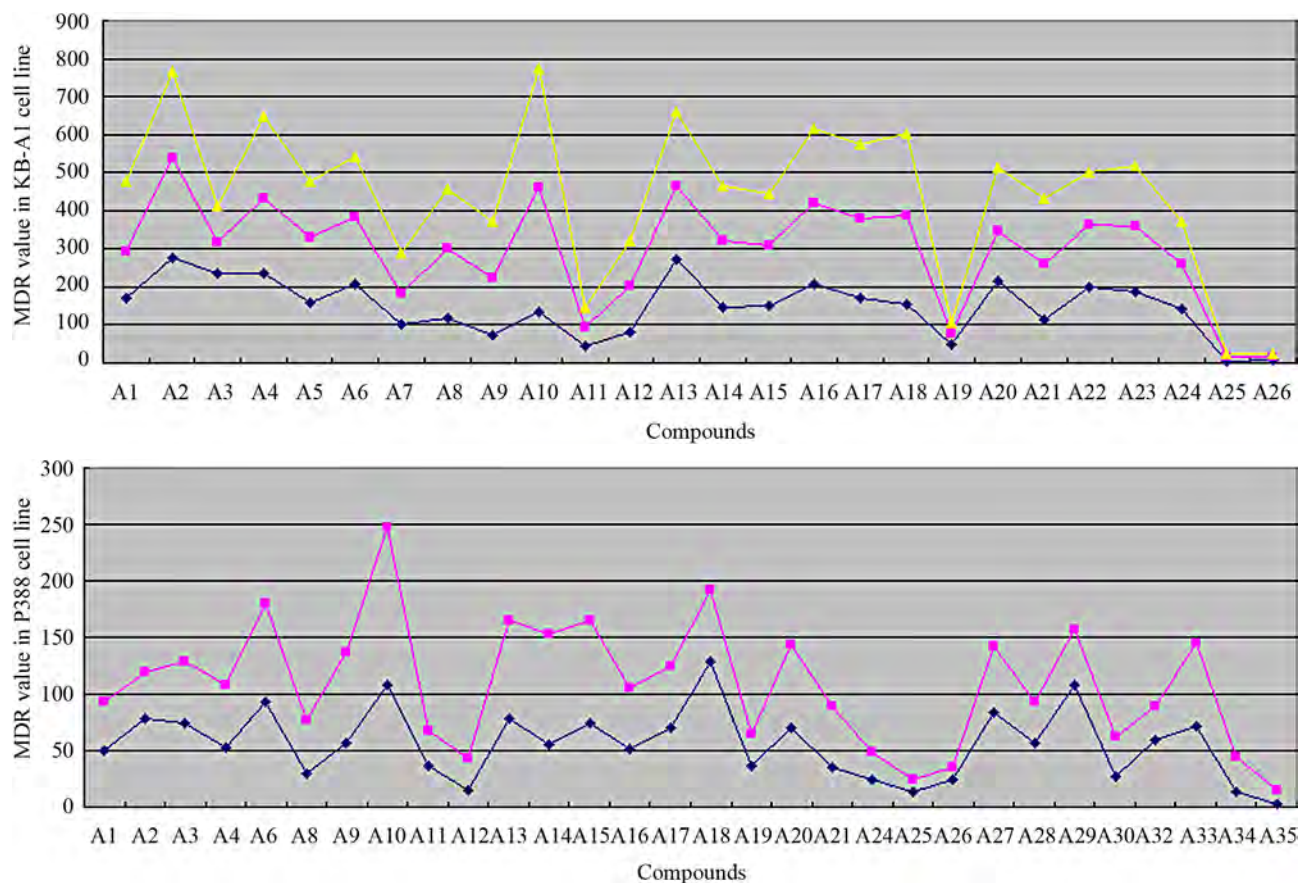


Figure 2. Comparison of the experimental MDR values with the corresponding predicted MDR values. Upper: MDR value in KB-A1/ADR cell lines (blue rhombic dots); MDR as predicted by Eq.4 MLR model (red square dots) and by Eq.5 MLR model (yellow triangle dots) for all the molecules of the training and test set. Down: MDR value in P388/VDR cell lines (blue rhombic dots); MDR as predicted by the method of PLSR (Eq.6) (red square dots) for all the molecules of the training and test set. The rhombic dots represented the experimental values (P388) and the predicted values of MDR, respectively.

Table 6. Comparison of experimental value of MDR ratio with predicted value of MDR ratio by PLSR.

No.	MDR (P388)	Pred MDR	LogP	MR	E _{VDW}	ShA	WI	No.	MDR (P388)	Pred MDR	LogP	MR	E _{VDW}	ShA	WI
A1	50	43.66	3.33	15.85	32.21	37.03	5476	A18	129	62.87	2.13	15.90	27.08	37.03	5476
A2	78	40.71	2.59	15.10	21.84	35.08	4872	A19	36	29.48	1.61	15.13	21.63	37.03	5585
A3	75	53.15	1.14	16.63	24.83	40.02	6522	A20	70	73.87	0.76	17.12	25.52	41.02	6855
A4	53	55.39	2.21	13.91	20.16	32.03	3916	A21	35	54.41	1.9	13.82	20.17	32.03	3874
A6	93	86.84	2.13	15.83	32.75	37.03	5476	A24	24	24.57	2.13	15.39	23.42	36.03	4855
A8	30	47.64	2.28	15.85	25.21	37.03	5476	A25	13	11.32	1.71	14.21	22.20	35.03	4487
A9	57	79.51	1.29	17.56	26.03	42.02	7353	A26	24	11.44	1.71	14.21	20.92	35.03	4538
A10	108	138.69	0.99	17.40	29.44	41.02	6935	A27	84	58.01	1.41	15.54	26.05	37.03	5476
A11	37	30.21	1.41	15.08	24.04	36.03	4909	A28	57	35.88	0.76	16.66	23.78	40.02	6244
A12	15	27.61	2.13	15.39	23.512	36.03	4909	A29	108	49.03	2.75	16.06	25.95	37.03	5476
A13	78	87.23	2.28	14.27	29.12	33.03	4216	A30	27	35.79	2.98	17.61	26.49	41.02	6804
A14	56	96.24	1.48	16.50	28.19	39.02	6288	A32	59	30.18	1.83	15.13	22.08	37.03	5642
A15	75	89.20	1.48	16.47	27.54	39.02	6288	A33	71	73.84	0.86	15.79	27.62	38.03	5822
A16	51	54.90	2.13	15.88	25.61	37.03	5476	A34	13	31.95	2.58	15.64	25.36	37.03	5476
A17	70	54.43	2.13	15.88	25.49	37.03	5476	A35	3	12.22	1.71	14.21	20.40	35.03	4589

the result of predicted value was in **Table 5**.

$$\text{LogMDR} = -6.537 + 7.162 \text{ LogMR} \\ N = 27; R = 0.445; F = 6.187 \quad (1)$$

$$\text{LogMDR} = -37.830 + 48.862 \text{ LogMR} - 0.499 \text{ ShA} \\ N = 27; R = 0.889; F = 45.415 \quad (2)$$

$$\text{LogMDR} = -35.816 + 52.416 \text{ LogMR} - 0.717 \text{ ShA} + \\ 6.612 \times 10^{-7} \text{ BI} \\ N = 27; R = 0.919; F = 41.442 \quad (3)$$

$$\text{LogMDR} = -38.791 + 56.923 \text{ LogMR} - 0.769 \text{ ShA} + \\ 5.897 \times 10^{-7} \text{ BI} - 0.159 \text{ LogP} \\ N = 27; R = 0.927; F = 33.504 \quad (4)$$

$$\text{LogMDE} = -42.192 + 61.818 \text{ LogMR} - 0.801 \text{ ShA} + \\ 4.791 \times 10^{-7} \text{ BI} - 0.369 \text{ LogP} + 3.595 \times 10^{-2} E_{\text{hyd}} \\ N = 27; R = 0.936; F = 29.749 \quad (5)$$

$$\text{LogMDR} = 7.611 + 3.138 \times 10^{-2} \text{ LogP} - 0.245 \text{ MR} + \\ 0.495 E_{\text{VDW}} - 0.509 \text{ ShA} + 8.802 \times 10^{-4} \text{ WI} \\ N = 30; Q^2 = 0.4650 \quad (6)$$

3.2. QSAR Analysis Based on Ka of ATPase in CCRF ADR5000 Cell Lines

Meanwhile, took Ka of ATPase of compounds in CCRF ADR5000 cell lines as dependent variable. Some QSAR models of a training set of 16 compounds were built using MLD method (Eqs.7-11) and PLSR method (Eq.12) (see **Figure 3**). All the molecular descriptors were listed in **Table 7**. A test set of 2 compounds was evaluated using the models as part of a validation process. **Table 8** displays the comparison of the experiment Ka and prediction Ka values of ATPase.

$$\text{LogKa} = 2.424 - 0.484 \text{ LogP} \\ N = 16; R = 0.860; F = 39.748 \quad (7)$$

$$\text{LogKa} = 3.612 - 0.285 \text{ LogP} - 0.0732 \text{ ShA} \\ N = 16; R = 0.900; F = 27.676 \quad (8)$$

$$\text{LogKa} = 2.573 - 0.480 \text{ LogP} - 0.285 \text{ ShA} + 0.651 \text{ MR} \\ N = 16; R = 0.914; F = 20.251 \quad (9)$$

$$\text{LogKa} = 7.313 - 0.752 \text{ LogP} - 0.647 \text{ ShA} + 1.642 \\ \text{MR} + 0.605 E_{\text{HOMO}} \\ N = 16; R = 0.928; F = 17.111 \quad (10)$$

$$\text{LogKa} = 10.021 - 0.875 \text{ LogP} - 1.044 \text{ ShA} + 2.263 \\ \text{MR} + 0.673 E_{\text{HOMO}} + 6.734 \times 10^{-4} \text{ WI} \\ N = 16; R = 0.945; F = 16.832 \quad (11)$$

$$\text{LogKa} = 3.662 - 0.279 \text{ LogP} - 4.71 \times 10^{-3} \text{ MW} + \\ 1.223 \times 10^{-2} E_{\text{HOMO}} \\ N = 18, Q^2 = 0.7100 \quad (12)$$

3.3. QSAR Analysis Based on BBB Partitioning of Organic Compounds

On the other hand, 37 organic compounds of training set and 8 compounds of test set were built and minimized, dissolved in liquid, and optimized by Monte Carlo method. Molecular modeling of the compound-membrane-water complex model revealed that the energy of an organic compound inserted at the middle position in the DMPC model with a layer of water was lower than that of the other two positions. Molecular descriptors of compounds in a training set and a test set are listed in **Table 9**. Six QSAR equations were constructed based on **Table 9** and were listed as follows.

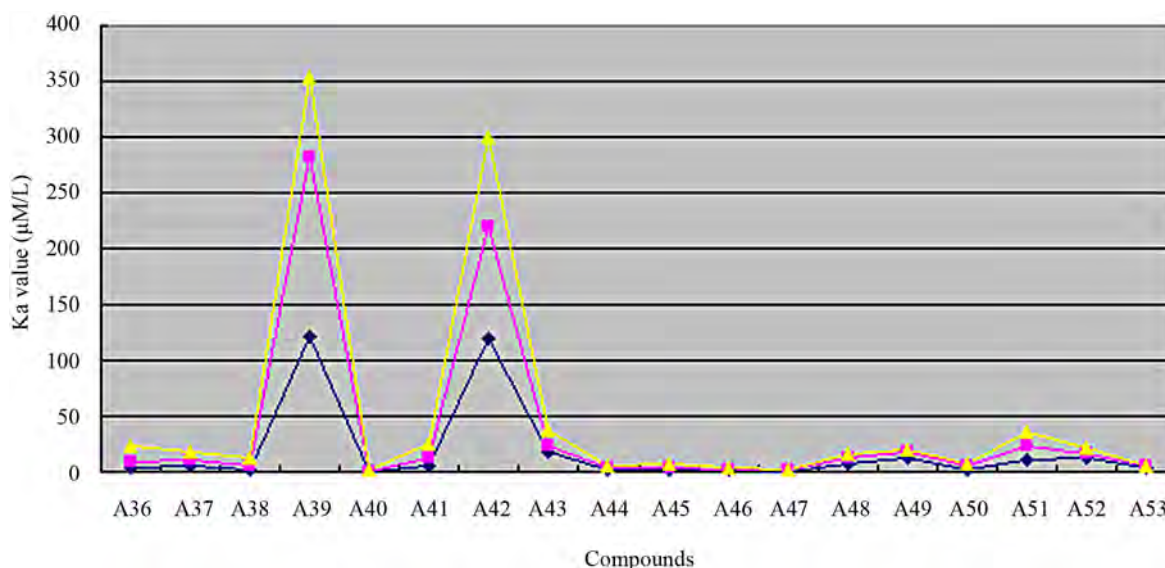


Figure 3. Comparison of the experimental Ka value (blue rhombic dots) with the corresponding predicted Ka as predicted by **Eq.11** MLR model (red square dots) and by **Eq.12** PLSR model (yellow triangle dots) for all the molecules of the training and test.

Table 7. The molecular descriptors of some compounds related to ATPase in the training/test sets.

No.	LogP	ShA	MR	E _{НОМО} (eV)	WI	MW	No.	LogP	ShA	MR	E _{НОМО} (eV)	WI	MW
A36	3.39	21.04	9.254	-9.14	1366	312.41	A45	4.3	26.04	11.42	-9.17	2345	383.53
A37	3.62	24.04	10.55	-9.20	1949	355.48	A46	4.93	32.03	13.27	-8.24	4689	462.57
A38	3.67	25.04	10.84	-9.16	2172	367.49	A47	5.2	32.03	13.38	-8.19	4329	464.58
A39	1.42	18.05	7.86	-9.12	920	277.37	A48	4.25	26.04	11.45	-9.24	2607	383.53
A40	4.93	32.03	13.27	-8.16	4329	462.57	A49	4.52	26.04	11.59	-8.94	2367	385.55
A41	2.67	25.04	10.29	-8.15	2244	372.44	A50	4.88	27.03	12.06	-8.94	2550	399.58
A42	0.94	19.05	8.01	-9.15	1050	293.37	A51	2.38	26.04	10.99	-9.09	2400	383.49
A43	2.54	25.04	10.52	-9.20	2172	369.46	A52	3.94	25.04	10.95	-9.05	2172	369.51
A44	3.98	32.03	13.50	-9.16	4227	459.59	A53	4.93	32.03	13.27	-8.19	4509	462.57

Table 8. Comparison the experimental values with the predictive values of Ka of these compounds.

No.	Ka (μM/L)	Predictive values of Ka						No.	Ka (μM/L)	Predictive values of Ka					
		Eq.7	Eq.8	Eq.9	Eq.10	Eq.11	Eq.12			Eq.7	Eq.8	Eq.9	Eq.10	Eq.11	Eq.12
A36	3.34	6.07	12.75	9.37	6.43	6.14	13.57	A45	1.53	2.20	3.02	3.32	2.69	2.08	3.50
A37	5.30	4.70	6.62	7.10	6.19	5.60	7.33	A46	1.47	1.09	0.73	0.52	0.48	0.81	1.02
A38	2.59	4.44	5.41	5.36	3.98	3.06	6.24	A47	0.55	0.81	0.61	0.46	0.50	0.53	0.84
A39	122	54.54	76.92	73.09	90.64	160.46	70.37	A48	7.64	2.33	3.13	3.83	3.33	4.22	3.60
A40	0.36	1.09	0.73	0.52	0.53	0.51	1.02	A49	12.20	1.72	2.62	3.39	4.98	5.00	2.99
A41	6.13	13.54	10.43	7.17	11.79	7.23	11.56	A50	2.26	1.15	1.75	2.37	3.50	3.28	2.04
A42	120.00	93.12	89.09	81.21	80.47	99.37	80.44	A51	10.50	18.71	10.66	14.57	16.6	13.20	12.02
A43	18.50	15.65	11.36	11.73	8.26	5.56	12.59	A52	12.80	3.29	4.53	4.74	4.57	3.91	5.15
A44	1.01	3.15	1.36	2.10	1.66	2.13	1.88	A53	4.15	1.09	0.73	0.52	0.51	0.65	1.02

Table 9. The molecular descriptors of the compounds related to BBB in the training/test sets.

No	PSA (Å ²)	ClogP	BI (Å)	E _{stretch} (Kcal/mol)	E _{total} ^a (Kcal/mol)	E _{torsion} ^a (Kcal/mol)	ΔE _{total} ^b (Kcal/mol)	ΔE _{torsion} ^b (Kcal/mol)
Training set								
B1	78.90	1.20	12378	-1.35503	-298.2972	-1713.1146	42.46	11.30
B2	94.00	1.99	1101758	-0.15595	-406.0803	-1789.8084	-65.32	-65.39
B3	73.00	3.80	1738650	-1.48472	-256.3021	-1703.1425	84.46	21.27
B4	87.00	1.63	1346396	-1.39112	-302.7543	-1841.5635	38.00	-117.15
B5	39.00	1.02	41807	0.58131	-226.3773	-1734.7452	114.38	-10.33
B6	26.80	3.23	305770	-0.09264	-228.2923	-1679.4604	112.47	44.96
B7	88.80	1.01	58510	0.71038	-279.0781	-1671.3414	61.68	53.07
B8	76.60	2.80	62216	-0.38334	-309.2981	-1654.6730	31.46	69.74
B9	104.40	1.77	83798	-0.35599	-313.4237	-1639.9898	27.34	84.43
B10	108.80	2.00	193593	-0.52172	-548.5593	-1640.9214	-207.80	83.49
B11	47.90	2.51	352512	-0.09496	-312.1226	-1656.7465	28.64	67.67
B12	45.20	4.27	779210	0.00479	-163.8011	-1716.3101	176.96	8.11
B13	38.50	2.61	158640	-0.09491	-170.3338	-1716.7159	170.43	7.70
B14	40.00	4.28	431722	-1.30506	-247.0951	-1748.0241	93.66	-23.61
B15	39.20	5.88	766256	0.09911	-289.2825	-1735.4004	51.48	-10.98
B16	54.90	5.14	766256	-0.14215	-181.0636	-1743.6068	159.70	-19.19
B17	18.80	0.62	20863	0.18071	-331.7044	-1695.6999	9.05	28.72

Continued

B18	46.70	0.27	20264	-1.36843	-209.4697	-1644.6752	131.29	79.74
B19	44.10	2.80	190375	-2.97778	-311.9182	-1713.8942	28.84	10.52
B20	5.40	4.85	210631	-0.06079	-235.7250	-1704.3399	105.03	20.08
B21	0.00	-0.47	4	0.00000	-407.3194	-1729.3793	-66.56	-4.96
B22	0.00	2.14	972	-0.00009	-239.8807	-1675.1827	100.88	49.23
B23	23.40	0.07	213	0.00000	-160.1278	-1672.3898	180.63	52.03
B24	22.60	0.69	712	0.00000	-319.0674	-1742.6968	21.69	-18.28
B25	0.00	3.74	1899	0.00067	-282.3721	-1751.6193	58.39	-27.20
B26	0.00	3.61	1661	0.00000	-285.7132	-1731.9518	55.05	-7.54
B27	0.00	1.43	1661	-0.00008	-238.7249	-1731.3090	102.03	-6.89
B28	0.00	2.48	633	0.00003	-291.5583	-1725.7370	49.20	-1.32
B29	11.60	2.46	21380	-0.00005	-418.0323	-1682.7138	-77.27	41.70
B30	24.40	-0.24	47	0.00000	-329.3150	-1704.6187	11.44	19.80
B31	10.70	1.27	7864	-0.00002	-253.3453	-1747.7044	87.41	-23.29
B32	0.00	2.37	7322	-0.00003	-268.8335	-1714.2486	71.93	10.17
B33	0.00	3.31	931	0.02567	-353.8395	-1739.7672	-13.08	-15.35
B34	24.40	-0.24	47	0.00000	-187.4520	-1720.5500	153.31	3.87
B35	0.00	1.93	7322	-0.00003	-177.4875	-1728.8621	163.27	-4.45
B36	0.00	2.64	2050	-0.02344	-220.3940	-1681.1548	120.36	43.26
B37	0.00	2.63	712	-0.00002	-231.5752	-1722.2582	109.18	2.16
Test set								
T1	22.70	0.321	712	0.00000	-274.7201	-1713.7409	66.04	10.68
T2	0.00	3.738	1838	0.00000	-225.6308	-1716.6234	115.13	7.79
T3	0.00	4.267	4150	0.00000	-331.3754	-1700.6397	9.38	23.78
T4	11.30	0.870	791	0.00000	-181.5954	-1700.8447	159.16	23.57
T5	0.00	4.397	4650	0.00000	-404.2903	-1741.2420	-63.53	-16.83
T6	0.00	1.103	0	0.00000	-282.9386	-1746.1889	57.82	-21.77
T7	0.00	3.339	791	0.00063	-271.9174	-1681.9440	68.84	42.47
T8	22.70	-0.208	213	0.00000	-364.8884	-1695.3605	-24.13	29.06

Note: ^aE_{total} and E_{torsion} mean the total energy and the torsion energy of the compound-DMPC-water complex; ^bΔE_{total} and ΔE_{torsion} are the residues between the compound-DMPC-water complex and the DMPC-water complex.

$$\log BB = 0.552 - 1.73 \times 10^{-2} PSA \quad n = 37 \quad R = 0.947 \quad S = 0.248 \quad (17)$$

$$n = 37 \quad R = 0.835 \quad S = 0.398 \quad (13)$$

$$\log BB = 0.229 - 1.70 \times 10^{-2} PSA + 0.131 C \log P \quad (14)$$

$$n = 37 \quad R = 0.878 \quad S = 0.352 \quad (14)$$

$$\log BB = 4.965 \times 10^{-2} - 1.28 \times 10^{-2} PSA + 0.211 C \log P - 6.40 \times 10^{-7} BI \quad (15)$$

$$n = 37 \quad R = 0.924 \quad S = 0.285 \quad (15)$$

$$\log BB = 6.262 \times 10^{-2} - 1.36 \times 10^{-2} PSA + 0.205 C \log P - 7.11 \times 10^{-7} BI - 0.185 E_{\text{stretch}} \quad (16)$$

$$n = 37 \quad R = 0.938 \quad S = 0.264 \quad (16)$$

$$\log BB = 6.580 \times 10^{-2} - 1.21 \times 10^{-2} PSA + 0.206 C \log P - 7.77 \times 10^{-7} BI - 0.197 E_{\text{stretch}} + 1.330 \times 10^{-3} \Delta E_{\text{total}} \quad (18)$$

$$\log BB = 8.730 \times 10^{-2} - 1.04 \times 10^{-2} PSA + 0.222 C \log P - 9.60 \times 10^{-7} BI - 0.183 E_{\text{stretch}} + 1.364 \times 10^{-3} \Delta E_{\text{total}} - 2.68 \times 10^{-3} \Delta E_{\text{torsion}} \quad (18)$$

$$n = 37 \quad R = 0.955 \quad S = 0.232 \quad (18)$$

Here, *n* means the number of compounds in a training set, *R* means the correlative coefficient, and *S* means the standard residual error. LogBB = log(C_{brain}/C_{blood}). PSA means the total polar surface area of a molecule. CLogP and BI display calculated LogP and connective index of molecular average total distance (relative covalent radius), respectively. They come from CS calculation. ΔE_{total} and ΔE_{torsion} are related to interaction between a compound and the membrane-water model. The total energy

and the torsion energy of the membrane-water complex are -340.7589 and -1724.4164 (Kcal/mol), respectively. ΔE_{total} is the change in the total potential energy of the solute-membrane-water complex comparing with that of the membrane-water model and so is $\Delta E_{\text{torsion}}$.

With the increase of the independent variable, the relativity of QSAR model was also improved and its predictive ability was enhanced. The most significant **Eq.18** displayed that the capability of a compound through BBB was directly proportional to ClogP and ΔE_{total} , but inversely proportional to PSA, BI, E_{stretch} , and $\Delta E_{\text{torsion}}$. **Figure 4** showed the comparison of the experimental logBB with the corresponding predicted logBB of the molecules in the training set based on **Eqs.17** and **18** models (see **Table 10**). Compound B18 was predicted with a higher logBB than observed, supported by the result of Iyer *et al.* [35].

The test set of 8 compounds to span almost the entire range in BBB partitioning was selected for validation of the QSAR models mentioned above. The observed and predicted logBB values for this test set were given in **Table 10** and plotted in **Figure 4** (right). It seemed to suggest that **Eqs.17** and **18** models could predict logBB

for other compounds in drug design.

4. DISCUSSION

Some predictive models of MDR, K_a and BBB partitioning of organic compounds were built by simulating the interaction between modulators or drugs and P-gp and/or the interreaction of the organic compound with the phospholipide-rich regions of cellular membranes. We have constructed theoretical models of the interaction between organic compounds and P-gp and compounds with the affinity for and simulation of the P-gp ATPase. On one hand, the interaction between compounds and P-gp (P-gp binding or MDR-reversal activity of compounds) is found to depend on LogP, LogMR, and ShA of compounds it transports, which proportional to LogMR whereas inversely proportional to LogP and ShA (see **Eqs.1-5**). Moreover, modulators or drugs interacting with P-gp and thus reducing the efflux of the cytotoxic compounds would increase the apparent toxicity of the cytotoxic compounds, which might account for more than one mechanism of action in the resistant cells used. There were many uncertainty factors in the MDR ratio assay method which was convinced by our linear

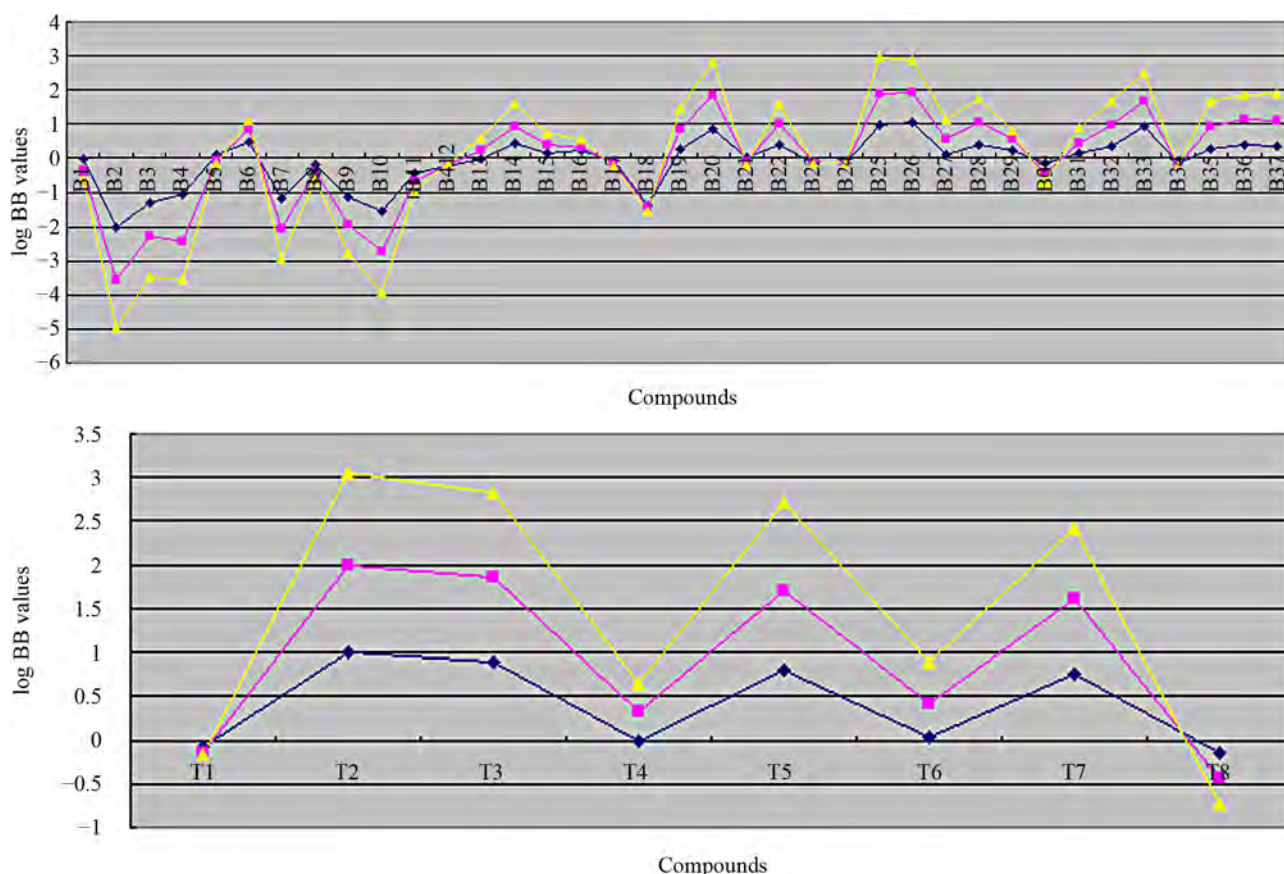


Figure 4. Comparison of the experimental logBB values (blue rhombic dots) for all the molecules of the training sets (upper) or the test set (down) to the corresponding predicted logBB as predicted by **Eq.17** MI-QSAR model (red square dots) and by **Eq.18** MI-QSAR model (yellow triangle dots).

Table 10. The experimental values and the predictive values of Log BB of these compounds.

No	Log BB	Predictive Value of log BB						No	Log BB	Predictive Value of log BB					
		Eq.13	Eq.14	Eq.15	Eq.16	Eq.17	Eq.18			Eq.13	Eq.14	Eq.15	Eq.16	Eq.17	Eq.18
Training set															
B1	-0.04	-0.81	-0.95	-0.71	-0.52	-0.33	-0.20	B20	0.85	0.46	0.77	0.87	0.85	0.99	1.01
B2	-2.00	-1.07	-1.11	-1.44	-1.56	-1.57	-1.39	B21	0.03	0.55	0.17	-0.05	-0.03	-0.12	-0.10
B3	-1.30	-0.71	-0.51	-1.20	-1.11	-0.98	-1.17	B22	0.37	0.55	0.51	0.50	0.50	0.64	0.57
B4	-1.06	-0.95	-1.04	-1.58	-1.49	-1.37	-1.13	B23	-0.15	0.15	-0.16	-0.23	-0.24	0.04	-0.03
B5	0.11	-0.12	-0.30	-0.26	-0.40	-0.19	-0.06	B24	-0.17	0.16	-0.06	-0.09	-0.10	-0.04	0.08
B6	0.49	0.09	0.20	0.19	0.16	0.34	0.28	B25	0.97	0.55	0.72	0.84	0.83	0.91	1.07
B7	-1.17	-0.98	-1.15	-0.91	-1.11	-0.90	-0.86	B26	1.04	0.55	0.70	0.81	0.80	0.88	0.98
B8	-0.18	-0.77	-0.71	-0.38	-0.38	-0.22	-0.22	B27	0.08	0.55	0.42	0.35	0.35	0.49	0.56
B9	-1.15	-1.25	-1.31	-0.97	-0.99	-0.79	-0.81	B28	0.40	0.55	0.55	0.57	0.57	0.64	0.71
B10	-1.57	-1.33	-1.36	-1.05	-1.05	-1.16	-1.20	B29	0.24	0.35	0.35	0.41	0.39	0.31	0.27
B11	-0.46	-0.28	-0.26	-0.26	-0.31	-0.21	-0.32	B30	-0.16	0.13	-0.22	-0.31	-0.32	-0.26	-0.26
B12	-0.24	-0.23	0.02	-0.13	-0.23	0.03	0.04	B31	0.13	0.37	0.21	0.18	0.17	0.31	0.43
B13	-0.02	-0.11	-0.08	0.01	-0.02	0.26	0.34	B32	0.35	0.55	0.54	0.55	0.54	0.64	0.68
B14	0.44	-0.14	0.11	0.17	0.33	0.51	0.64	B33	0.93	0.55	0.66	0.75	0.74	0.73	0.84
B15	0.14	-0.13	0.33	0.30	0.17	0.26	0.33	B34	-0.16	0.13	-0.22	-0.31	-0.32	-0.07	-0.02
B16	0.22	-0.40	-0.03	-0.06	-0.15	0.10	0.22	B35	0.27	0.55	0.48	0.45	0.45	0.68	0.74
B17	-0.06	0.23	-0.01	-0.07	-0.11	-0.07	-0.09	B36	0.37	0.55	0.57	0.61	0.61	0.77	0.72
B18	-1.40	-0.26	-0.53	-0.50	-0.28	-0.02	-0.14	B37	0.34	0.55	0.57	0.60	0.60	0.75	0.81
B19	0.25	-0.21	-0.15	-0.05	0.45	0.59	0.62								
Test set															
T1	-0.08	0.16	-0.11	-0.17	-0.18	-0.06	-0.02	T5	0.81	0.55	0.81	0.97	0.96	0.88	1.02
T2	1.01	0.55	0.72	0.84	0.83	0.99	1.05	T6	0.04	0.55	0.37	0.28	0.29	0.37	0.47
T3	0.90	0.55	0.79	0.95	0.93	0.95	0.98	T7	0.76	0.55	0.67	0.75	0.75	0.84	0.81
T4	0.00	0.36	0.15	0.09	0.09	0.32	0.32	T8	-0.15	0.16	-0.18	-0.28	-0.29	-0.28	-0.31

regression models. Our research results using two different statistic methods, MLR and PLSR, have revealed that the QSAR equation was also improved and the predictive ability of the models was enhanced with the increase of the variable. **Eq.5** was built on KB-A1 cell line with a cytotoxic compound of 2.5 μM ADR while **Eq.6** was based on P388/VDR-20 cell line with 1.5 μM VCR. Here, most of the models gave satisfactory cross-validated Q^2 above 0.500, conventional R above 0.800 and less SE values, indicating their proper predictive ability. Significant differences between values were examined using two-tailed paired T test provided by SPSS. All the results were considered not significant if $P < 0.05$. **Eq.5** model was the most significant and indicated that the potential of P-gp modulators interacted with P-gp depended upon MR, BI, E_{hyd} , ShA, and LogP. The former three displayed positive contributions to the MDR activity of P-gp, suggesting that the MDR activity increased accordingly with the increase of MR. The latter two displayed negative contribution to the MDR activity of P-gp.

On the other hand, our built models for Ka of ATPase based on the analogies of purine and propafenone analogs suggested that the enzyme hydrolysis of these compounds largely depended on LogP, MR, ShA, MW and E_{HOMO} , especially positive related to MR but negative to LogP and ShA (see **Eqs.7 to 11**). Both models, **Eq.11** by MLR and **Eq.12** by PLSR, pointed out that E_{HOMO} , positive related with the activity of P-gp ATPase, was an important parameter for the compound stimulated ATPase activity with high affinity, whereas another LogP was negative related with the activity of P-gp ATPase. **Figure 3** showed that molecular A39 and A42 with higher Ka value of ATPase were depart from other compounds. This may be because they have lower lipophilicity, which is supported by the research results of Diethart Schmid *et al.* [31]. The results above showed that the P-gp binding capacity of these compounds shares common characteristics with their ATPase hydrolysis, namely their hydrophobic parameters (such as logP) and steric parameters (e.g. MW, ShA, and MR).

In another aspect, our MI-QSAR models indicated that the distribution of organic molecules through BBB was not only influenced by organic solutes themselves, but also related to the properties of the solute-membrane-water complex, namely interactions of the molecule with the phospholipide-rich regions of cellular membranes. The QSAR model, especially **Eq.18** most significant, revealed that the capability of BBB partitioning of an organic compound focused on six significant features. Obviously, two descriptors, ClogP and ΔE_{total} , had positive regression coefficients and the other four descriptors, PSA, BI, E_{stretch} , and $\Delta E_{\text{torsion}}$, had negative regression coefficients. Moreover, PSA descriptor was found as a

dominant descriptor in these QSAR models, which was related to the aqueous solubility of the solute compound along with a direct lipophilicity descriptor. When the value of PSA of a molecule lessened within the range from 0 to 108.80 \AA^2 , its value of LogBB would increase. This was consistent with the experimental results that the more polarity it possessed, the more difficultly a molecule entered the hydrophobic environment of BBB [38]. BI as the connective index of molecular average total distance pertained to the volume parameter. Our research result showed that a molecule more and more difficultly crossed through BBB by diffusion with the addition of its bulk. However, the value of LogBB of a molecule increased with the increase of ClogP. It meant that the hydrophobic molecule could pass through BBB more easily than the hydrophilic molecule does. The presence of E_{stretch} descriptor suggested that with the decrease of the stretch-bend energy of a molecule, its value of LogBB increased. Two of the descriptors, ΔE_{total} and $\Delta E_{\text{torsion}}$, found in the logBB QSAR models (**Eqs.17 and 18**), reflected the behavior of the solutes in the membrane and the entire membrane-solute complex. Along with the meaning mentioned, ΔE_{total} was equivalent to the change in the average total potential energy between the ternary complex of solute-membrane-water and the binary complex of membrane-water. Similarly, $\Delta E_{\text{torsion}}$ was the difference between the dihedral torsion energy of the ternary complex and that of the binary complex. Here, the more the change value of ΔE_{total} was, the more its value of LogBB increased. This may be because small molecules across BBB membrane could lead to the change of the complex structure. The more changeability of the structure resulted in greater change of the total potential energy, while the addition of the energy change could be the important cause of the increase of the capability of a small molecule through BBB. On the contrary, the less the difference of the torsion energy was, the larger its LogBB value was. It displayed that a small molecule tight combined with the membrane-water complex could lead to the increase of its LogBB. Moreover, the relationship would suggest that the solute became more flexible within the membrane-water complex, which would possess the greater logBB value, in agreement with the research results of Iyer M *et al.* [35]. Furthermore, BBB partitioning was mainly found to depend upon two parameters, namely PSA and ClogP, where the ability of organic molecules permeating across BBB was directly proportional to LogP but inversely proportional to PSA (see **Eqs.13-18**), which was consistent with the research results of Chen and co-worker [2], namely the increasing PSA decreased LogBB rapidly while LogP was positively related to LogBB. It indicated that molecules with higher lipophilic would be partitioned into the lipid bilayer more easily with more chances to penetrate BBB, sup-

ported by the research result of Wang *et al.*, namely a large number of structurally and functionally diverse compounds as substrates or modulators of P-gp mostly sharing common structural features, such as aromatic ring structures and high lipophilicity [19]. PSA of CNS active drug should be lower than 90 \AA^2 [2], while the penetration through the BBB is optimal for LogP value in the range 1.5 - 2.7 (Norinder & Haeberlein, 2002).

In addition, several non-MI-QSAR computational models to describe and predict BBB partitioning have been reported that includes other descriptors besides PSA and ClogP [39]. An alternative, complementary approach to BBB partitioning prediction uses MI-QSAR analysis developed by Iyer M *et al.* [35]. Their research results showed that BBB partitioning of an organic compound depended upon PSA, CLogP, and the conformational flexibility of the compounds as well as the strength of their "binding" to the model biologic membrane. The MI-QSAR models indicated that BBB partitioning process could be reliably described for structurally diverse molecules and provided interactions of the molecule with the phospholipide-rich regions of cellular membranes. An extension of these approaches that combined QSAR with solute-membrane-water complex had been developed by us, which was addition of a layer of water on the hydrophilic side of DMPC monolayer membrane in order to simulate the truth BBB environment. Our results revealed that the distribution of organic molecules through BBB was not only influenced by the properties of organic solutes, but also related to the property of the solute-membrane-water complex. The former involved the polarity, hydrophobic, size, and conformational freedom degree of organic molecules, while the latter dealt with the strength of an organic molecule combined with BBB membrane and the structural changeability of a solute-membrane-water complex. Furthermore, the capability of a small molecule across BBB was mainly related to four physicochemical factors, which depended on the relative polarity of a small molecule (namely PSA and ClogP), the molecular volume (*i.e.* BI), the strength of a small molecule combined with DMPC-water model (*viz.* $\Delta E_{\text{torsion}}$), and the changeability of the structure of a solute-membrane-water complex (*scilicet* ΔE_{total}). The QSAR model showed that the less polarity and more hydrophobic molecules relatively easily passed through BBB and entered brain to cure. The reason for the change of the total energy was that small molecules across BBB membrane caused the structural change of the solute-membrane-water complex. The more the changeability of the complex structure was, the more the change value of its total energy was, and the more easily a small molecule penetrated BBB.

In particular, cerebral clearance of $A\beta$ was considered to occur via elimination across BBB, as well as prote-

olytic degradation. Attenuation of its elimination was likely to result in the increase of cerebral $A\beta$ deposition, which may facilitate progression of AD [40]. P-gp detoxified cells by exporting hundreds of chemically unrelated toxins but had been implicated in MDR in the treatment of cancers. Substrate promiscuity was a hallmark of P-gp activity, thus a structural description of poly-specific drug-binding was important for the rational design of anti-amyloid accumulation drugs, anticancer drugs and MDR inhibitors. The x-ray structure of apo P-gp at 3.8 angstroms revealed an internal cavity of approximately 6000 \AA^3 with a 30 \AA separation of the two nucleotide-binding domains. Two additional P-gp structures with cyclic peptide inhibitors demonstrated distinct drug-binding sites in the internal cavity capable of stereoselectivity that was based on hydrophobic and aromatic interactions. Apo and drug-bound P-gp structures had portals open to the cytoplasm and the inner leaflet of the lipid bilayer for drug entry. The inward-facing conformation represented an initial stage of the transport cycle that was competent for drug binding [41]. Currently, P-gp was identified as an energy-dependent pump, whereas ATPase activity as an assay in itself was possibly problematical because the assay was based upon one assumption that drug-induced ATP hydrolysis reflects transport by the transporter [16]. There may be many ways in which this activity could be altered, including direct action on the ATP binding domain. Scientists once observed some compounds such as daunomycin and vinblastine inhibit ATPase activity, but increase in others, suggesting that modulation of ATPase activity was highly dependent on experimental conditions and may not correlate well with the ability of P-gp to transport the drug [42-44]. The work of Litman *et al.* was one of the few studies suggesting that affinity between drugs and ATPase activity has no correlation to LogP, but Surface Area [45]. Because of the less comparability of molecular structures in a training set, our QSAR model possessed more universal significance. However, the precision of the QSAR models was so low that there was still a distance to its application. So a series of organic compounds with similar structures are chosen and consist of a training set, thus the precision of QSAR simulation will be largely increased, while the prediction of the analogues through BBB will be greatly improved.

5. CONCLUSIONS

The pathogenesis of AD is characterized by the aggregation of $A\beta$ into neurotoxic plaques. P-gp is involved in MDR and in neurodegenerative disorders such as PD, AD and epilepsy. P-gp mediates the efflux of $A\beta$ from the brain as well as mediates MDR, while P-gp transports neutral or positively-charged hydrophobic sub-

strates with consuming energy from ATP hydrolysis. In comparison with the ability of organic molecules permeating across BBB, P-gp binding or MDR-reversal activity of compounds has a negative correlation with LogP. Moreover, P-gp binding or MDR-reversal activity of compounds is mainly proportional to LogMR (Eqs.1 to 5) but inversely proportional to LogP (Eqs.4 and 5). Similarly, ATPase activity of these compounds was largely negatively related to LogP (Eqs.7 to 12) but positively related to MR (Eqs.9 to 11), where most compounds are with logP value more than 2.7. This showed that the P-gp binding capacity of these compounds shared common characteristics with their ATPase hydrolysis, namely their hydrophobic parameters (*i.e.* logP) and steric parameters (e.g. MR). Additionally, the distribution of organic molecules through BBB was not only influenced by organic solutes themselves, but also related to the properties of the solute-membrane water complex, namely interactions of the molecule with the phospholipide-rich regions of cellular membranes. The ability of organic molecules permeating across BBB was mostly proportional to LogP (Eqs.14 to 18) but inversely proportional to PSA (Eqs.13 to 18), which is consistent with the research results of Chen and co-workers [2], namely the increasing PSA decreased LogBB rapidly while LogP positively related to LogBB. Chen *et al.* have indicated that the optimum logP for designing CNS active drug was about 2.9 and the compound with LogP lower than 2.9 had a positive correlation with logBB, but the compound with logP bigger than 2.9 made an unfavorable contribution [2]. It is disclosed that molecules with higher lipophilic would be partitioned into the lipid bilayer more easily with more chances to penetrate BBB, supported by the research result of Wang *et al.*, namely a large number of structurally and functionally diverse compounds as substrates or modulators of P-gp mostly share common structural features, such as aromatic ring structures and high lipophilicity [19]. The LogP not only offered opportunity to penetrate the lipid bilayer, but also gave favorable contribution to binding with P-gp or P450. There may be two reasons for this phenomenon. Firstly, the compounds with higher liposolubility are more vulnerable to cytochrome P450 metabolism, leading to faster clearance [46]. P450 enzymes catalyze the metabolism of a wide variety of endogenous and exogenous compounds including xenobiotics, drugs, environmental toxins, steroids, and fatty acids. Aminated thioxanthenes have recently been reported as P-gp inhibitors as well as its interaction with cytochrome P450 3A4 (CYP3A4), as many substrates of P-gp and CYP3A4 are common [47], which could be a major cause of P-gp binding or MDR-reversal activity of compounds inversely proportional to LogP. The second reason was related to the mechanism of P-gp action. According to the model proposed by

Higgins and Gottesman [48], after entering into the phospholipid bilayer, compound may interact with P-gp in the inner leaflet of the lipid bilayer. Upon interaction with P-gp, the compound was flipped from the inner leaflet to the outer leaflet of the lipid bilayer. The lipophilic compounds with high LogP entered into cellular membrane easily and intended to retain there, so its opportunity to interact with P-gp increased and then its opportunity to be pumped out of cells enhanced.

In conclusion, the predictive model of BBB partitioning of organic compounds contributed to the discovery of potential AD therapeutic drugs. Moreover, the interaction model of P-gp and modulators for the treatment of multidrug resistance indicates the discovery of some molecules to increase A β clearance from the brain and reduce A β brain accumulation by regulating BBB P-gp in the early stages of AD. Because P-gp is a transporter whose ligands are almost exclusively small molecules, it is not surprising that the pump itself is unable to transport A β . Nazer and co-worker have indicated the non-proteolytic clearance of A β via receptor-mediated transport across the BBB and investigated P-gp and the low-density lipoprotein receptor-related protein (LRP) involving A β efflux across the BBB [49]. Nevertheless, LRP or P-gp alone was insufficient for non-proteolytic transcytosis of intact A β . LRP in transcytosing intact A β across the BBB may require a co-transporter, such as P-gp [49]. Elucidation of the molecular mechanisms of the potential of LRP and P-gp to efflux cortical A β across BBB should help to promote rational therapeutic strategy in AD.

6. ACKNOWLEDGEMENTS

This work was supported by a grant from Basic Scientific Research Expenses of Central University (020814360012), National Key Technology R&D Program (2008BAI51B01) and Specialized Research Fund for the Doctoral Program of Higher Education (20120091110038).

REFERENCES

- [1] Cheng, Z., Zhang, J., Liu, H., Li, Y., Zhao, Y. and Yang, E. (2010) Central nervous system penetration for small molecule therapeutic agents does not increase in multiple sclerosis- and Alzheimer's disease-related animal models despite reported blood-brain barrier disruption. *Drug Metabolism & Disposition*, **38**, 1355-1361. [doi:10.1124/dmd.110.033324](https://doi.org/10.1124/dmd.110.033324)
- [2] Chen, Y., Zhu, Q.J., Pan, J., Yang, Y. and Wu, X.P. (2009) A prediction model for blood-brain barrier permeation and analysis on its parameter biologically. *Computer Methods and Programs in Biomedicine*, **95**, 280-287. [doi:10.1016/j.cmpb.2009.03.006](https://doi.org/10.1016/j.cmpb.2009.03.006)
- [3] Miklossy, J. (2011) Alzheimer's disease—A neurospirochetosis. Analysis of the evidence following Koch's and

- Hill's criteria. *Journal of Neuroinflammation*, **8**, 90.
- [4] Inoue, M., Konno, T., Tainaka, K., Nakata, E., Yoshida, H.O. and Morii, T. (2012) Positional effects of phosphorylation on the stability and morphology of tau-related amyloid fibrils. *Biochemistry*, **51**, 1396-1406.
- [5] Daebel, V., Chinnathambi, S., Biernat, J., Schwalbe, M., Habenstein, B., Loquet, A., Akoury, E., Tepper, K., Müller, H., Baldus, M., Griesinger, C., Zweckstetter, M., Mandelkow, E., Vijayan, V. and Lange, A. (2012) β -sheet core of tau paired helical filaments revealed by solid-state NMR. *Journal of the American Chemical Society*, **134**, 13982-13989. doi:10.1021/ja305470p
- [6] Jeynes, B. and Provias, J. (2011) An investigation into the role of p-glycoprotein in Alzheimer's disease lesion pathogenesis. *Neuroscience Letters*, **487**, 389-393. doi:10.1016/j.neulet.2010.10.063
- [7] Vogelgesang, S., Jedlitschky, G., Brenn, A. and Walker, L.C. (2011) The role of the ATP-binding cassette transporter p-glycoprotein in the transport of β -amyloid across the blood-brain barrier. *Current Pharmaceutical Design*, **17**, 2778-2786. doi:10.2174/138161211797440168
- [8] Bartels, A.L. (2011) Blood-brain barrier p-glycoprotein function in neurodegenerative disease. *Current Pharmaceutical Design*, **17**, 2771-2777. doi:10.2174/138161211797440122
- [9] Gottesman, M.M. and Pastan, I. (1993) Biochemistry of multidrug resistance mediated by the multidrug transporter. *Annual Review of Biochemistry*, **62**, 385-427.
- [10] Kast, C., Canfield, V., Levenson, R. and Gros, P. (1996) Transmembrane organization of mouse p-glycoprotein determined by epitope insertion and immunofluorescence. *The Journal of Biological Chemistry*, **271**, 9240-9248.
- [11] Bendayan, R., Lee, G. and Bendayan, M. (2002) Functional expression and localization of p-glycoprotein at the blood brain barrier. *Microscopy Research and Technique*, **57**, 365-380.
- [12] Abuznait, A.H., Cain, C., Ingram, D., Burk, D. and Kadoumi, A. (2011) Up-regulation of p-glycoprotein reduces intracellular accumulation of beta amyloid: Investigation of p-glycoprotein as a novel therapeutic target for Alzheimer's disease. *Journal of Pharmacy and Pharmacology*, **63**, 1111-1118. doi:10.1111/j.2042-7158.2011.01309.x
- [13] Kothandan, G., Gadhe, C.G., Madhavan, T., Choi, C.H. and Cho, S.J. (2011) Docking and 3D-QSAR (quantitative structure activity relationship) studies of flavones, the potent inhibitors of p-glycoprotein targeting the nucleotide binding domain. *European Journal of Medicinal Chemistry*, **46**, 4078-4088. doi:10.1016/j.ejmech.2011.06.008
- [14] Hartz, A.M., Miller, D.S. and Bauer, B. (2010) Restoring blood-brain barrier p-glycoprotein reduces brain amyloid-beta in a mouse model of Alzheimer's disease. *Molecular Pharmacology*, **77**, 715-723. doi:10.1124/mol.109.061754
- [15] Jabeen, I., Pleban, K., Rinner, U., Chiba, P. and Ecker, G.F. (2012) Structure-activity relationships, ligand efficiency, and lipophilic efficiency profiles of benzophenone-type inhibitors of the multidrug transporter p-glycoprotein. *Journal of Medicinal Chemistry*, **55**, 3261-3273.
- [16] Stouch, T.R. and Gudmundsson, O. (2002) Progress in understanding the structure-activity relationships of p-glycoprotein. *Advanced Drug Delivery Reviews*, **54**, 315-328. doi:10.1016/S0169-409X(02)00006-6
- [17] Sharom, F.J. (1997) The p-glycoprotein efflux pump: How does it transport drugs? *The Journal of Membrane Biology*, **160**, 161-175. doi:10.1007/s002329900305
- [18] Li, Y., Wang, Y.H., Yang, L., Zhang, S.W., Liu, C.H. and Yang, S.L. (2005) Comparison of steroid substrates and inhibitors of p-glycoprotein by 3D-QSAR analysis. *Journal of Molecular Structure*, **733**, 111-118.
- [19] Wang, R.B., Kuo, C.L., Lien, L.L. and Lien, E.J. (2003) Structure-activity relationship: Analyses of p-glycoprotein substrates and inhibitors. *Journal of Clinical Pharmacy and Therapeutics*, **28**, 203-228.
- [20] Wang, Y.H., Li, Y., Yang, S.L. and Yang, L. (2005) An in silico approach for screening flavonoids as p-glycoprotein inhibitors based on a Bayesian-regularized neural network. *Journal of Computer-Aided Molecular Design*, **19**, 137-147. doi:10.1007/s10822-005-3321-5
- [21] Chen, C. and Yang, J. (2006) MI-QSAR models for prediction of corneal permeability of organic compounds. *Acta Pharmacologica Sinica*, **27**, 193-204. doi:10.1111/j.1745-7254.2006.00241.x
- [22] Kubinyi, H. (1995) Strategies and recent technologies in drug discovery. *Pharmazie*, **50**, 647-662.
- [23] Wiese, M. and Pajeva, I.K. (2001) Structure-activity relationships of multidrug resistance reversers. *Current Medicinal Chemistry*, **8**, 685-713.
- [24] Taub, M.E., Podila, L., Ely, D. and Almeida, I. (2005) Functional assessment of multiple p-glycoprotein (p-gp) probe substrates: Influence of cell line and modulator concentration on p-gp activity. *Drug Metabolism & Disposition*, **33**, 1679-1687. doi:10.1124/dmd.105.005421
- [25] Alka, K. (2003) C-QSAR: A database of 18000 QSARs and associated biological and physical data. *Journal of Computer-Aided Molecular Design*, **17**, 187-196.
- [26] Kuo, C.L., Assefa, H., Kamath, S., Brzozowski, Z., Slawinski, J., Saczewski, F., Buolamwini, J.K. and Neamati, N. (2004) Application of CoMFA and CoMSIA 3D-QSAR and docking studies in optimization of mercaptobenzenesulfonamides as HIV-1 integrase inhibitors. *Journal of Medicinal Chemistry*, **47**, 385-399. doi:10.1021/jm030378i
- [27] Cramer, R.D., Patterson, D.E. and Bunce, J.D. (1988) Comparative molecular field analysis (CoMFA). 1. Effect of shape on binding of steroids to carrier proteins. *Journal of the American Chemical Society*, **110**, 5959-5967.
- [28] Chen, L.J., Lian, G.P. and Han, L.J. (2007) Prediction of human skin permeability using artificial neural network (ANN) modeling. *Acta Pharmacologica Sinica*, **28**, 591-600.
- [29] Dhainaut, A., Regnier, G., Tizot, A., Pierre A., Leonce, S., Guilbaud, N., Kraus-Berthier, L. and Atassi, G. (1996) New purines and purine analogs as modulators of multidrug resistance. *Journal of Medicinal Chemistry*, **39**,

- 4099-4108.
- [30] Ford, J.M., Bruggemann, E.P., Pastan, I., Gottesman, M.M. and Hait, W.N. (1990) Cellular and biochemical characterization of thioxanthenes for reversal of multidrug resistance in human and murine cell lines. *Cancer Research*, **50**, 1748-1756.
- [31] Schmid, D., Ecker, G., Kopp, S., Hitzler, M. and Chiba, P. (1999) Structure-activity relationship studies of propafenone analogs based on p-glycoprotein ATPase activity measurements. *Biochemical Pharmacology*, **58**, 1447-1456. [doi:10.1016/S0006-2952\(99\)00229-4](https://doi.org/10.1016/S0006-2952(99)00229-4)
- [32] Karelson, M. (2000) Molecular descriptors in QSAR/QSPR. John Wiley & Sons, New York.
- [33] Karelson, M., Lobanov, V.S. and Katritzky, A.R. (1996) Quantum-chemical descriptors in QSAR/QSPR studies. *Chemical Reviews*, **96**, 1027-1044.
- [34] Ponce, Y.M., Garit, J.A., Torrens, F., Zaldivar, V.R. and Castro, E.A. (2004) Atom, atom-type, and total linear indices of the "molecular pseudograph's atom adjacency matrix": Application to QSPR/QSAR studies of organic compounds. *Molecules*, **9**, 1100-1123. [doi:10.3390/91201100](https://doi.org/10.3390/91201100)
- [35] Iyer, M., Mishra, R., Han, Y. and Hopfinger, A.J. (2002) Predicting blood-brain barrier partitioning of organic molecules using membrane-interaction QSAR analysis. *Pharmaceutical Research*, **19**, 1611-1621. [doi:10.1023/A:1020792909928](https://doi.org/10.1023/A:1020792909928)
- [36] Abraham, M.H., Chadha, H.S. and Mitchell, R.C. (1995) Hydrogen bonding. 36. Determination of blood-brain barrier distribution using octanol-water partition coefficients. *Drug Design and Discovery*, **13**, 123-131.
- [37] Abraham, M.H., Takacs-Novak, K. and Mitchell, R.C. (1997) On the partition of ampholytes: Application to blood-brain distribution. *Journal of Pharmaceutical Sciences*, **86**, 310-315. [doi:10.1021/js960328j](https://doi.org/10.1021/js960328j)
- [38] Bassolino-Klimas, D., Alper, H.E. and Stouch, T.R. (1993) Solute diffusion in lipid bilayer membranes: An atomic level study by molecular dynamics simulation. *Biochemistry*, **32**, 12624-12637. [doi:10.1021/bi00210a010](https://doi.org/10.1021/bi00210a010)
- [39] Ma, X.L., Chen, C. and Yang, J. (2005) Predictive model of blood-brain barrier penetration of organic compounds. *Acta Pharmacologica Sinica*, **26**, 500-512. [doi:10.1111/j.1745-7254.2005.00068.x](https://doi.org/10.1111/j.1745-7254.2005.00068.x)
- [40] Ohtsuki, S., Ito, S. and Terasaki, T. (2010) Is p-glycoprotein involved in amyloid- β elimination across the blood-brain barrier in Alzheimer's disease? *Clinical Pharmacology & Therapeutics*, **88**, 443-445.
- [41] Aller, S.G., Yu, J., Ward, A., Weng, Y., Chittaboina, S., Zhuo, R., Harrell, P.M., Trinh, Y.T., Zhang, Q., Urbatsch, I.L. and Chang, G. (2009) Structure of p-glycoprotein reveals a molecular basis for poly-specific drug binding. *Science*, **323**, 1718-1722. [doi:10.1126/science.1168750](https://doi.org/10.1126/science.1168750)
- [42] Ambudkar, S.V., Lelong, I.H., Zhang, J., Cardarelli, C.O., Gottesman, M.M. and Pastan, I. (1992) Partial purification and reconstitution of the human multidrug-resistance pump: Characterization of the drug-stimulatable ATP hydrolysis. *Proceedings of the National Academy of Sciences of the United States of America*, **89**, 8472-8476.
- [43] Shapiro, A.B. and Ling, V. (1994) ATPase activity of purified and reconstituted p-glycoprotein from Chinese hamster ovary cells. *The Journal of Biological Chemistry*, **269**, 3745-3754.
- [44] Doige, C.A., Yu, X. and Sharom, F.J. (1993) The effects of lipids and detergents on ATPase-active p-glycoprotein. *Biochimica et Biophysica Acta*, **1146**, 65-72.
- [45] Litman, T., Zeuthen, T., Skovsgaard, T. and Stein, W.D. (1997) Structure-activity relationships of p-glycoprotein interacting drugs: Kinetic characterization of their effects on ATPase activity. *Biochimica et Biophysica Acta*, **1361**, 159-168.
- [46] Waterhouse, R.N. (2003) Determination of lipophilicity and its use as a predictor of blood-brain barrier penetration of molecular imaging agents. *Molecular Imaging & Biology*, **5**, 376-389. [doi:10.1016/j.mibio.2003.09.014](https://doi.org/10.1016/j.mibio.2003.09.014)
- [47] Palmeira, A., Sousa, E., Fernandes, M.X., Pinto, M.M. and Vasconcelos, M.H. (2012) Multidrug resistance reversal effects of aminated thioxanthenes and interaction with cytochrome P450 3A4. *Journal of Pharmacy and Pharmaceutical Sciences*, **15**, 31-45.
- [48] Higgins, C.F. and Gottesman, M.M. (1992) Is the multidrug transporter a flippase? *Trends in Biochemical Sciences*, **17**, 18-21.
- [49] Nazer, B., Hong, S. and Selkoe, D.J. (2008) LRP promotes endocytosis and degradation, but not transcytosis, of the amyloid-beta peptide in a blood-brain barrier *in vitro* model. *Neurobiology of Disease*, **30**, 94-102. [doi:10.1016/j.nbd.2007.12.005](https://doi.org/10.1016/j.nbd.2007.12.005)